

Ultralight Dark Matter Constraints from NanoHertz Gravitational Waves

Shreyas Tiruvaskar^{1,*}, Russell Boey^{2,†}, Richard Easther^{2,‡} and Chris Gordon^{1,§}

¹*School of Physical and Chemical Sciences, University of Canterbury, New Zealand*

²*Department of Physics, University of Auckland, Private Bag 92019, Auckland, New Zealand*

(Dated: December 18, 2025)

We investigate the impact of ultralight dark matter (ULDM) on the mergers of supermassive black holes (SMBH) and the resulting stochastic gravitational wave background. ULDM is based on exceptionally light particles and yields galactic halos with dense central solitons. This increases the drag experienced by binary SMBH, decreasing merger times and potentially suppressing gravitational radiation from the binary at low frequencies. We develop semi-analytic models for the decay of SMBH binaries in ULDM halos and use current pulsar timing array (PTA) measurements to constrain the ULDM particle mass and its fractional contribution to the dark matter content of the universe. We find a median ULDM particle mass of $7. \times 10^{-22}$ eV and show that scaling relations suggest that the drag remains effective at relatively low ULDM fractions, which are consistent with all other constraints on the model. Consequently, future pulsar timing measurements will be a sensitive probe of any ULDM contribution to the overall dark matter content of the universe.

I. INTRODUCTION

Pulsar timing experiments provide direct evidence for the presence of a very low frequency gravitational wave background in the universe [1–5]. These observations are broadly consistent with the signal expected from binary supermassive black hole (SMBH) mergers that would follow the unions of their parent galaxies during the hierarchical growth of structure.

Gravitational wave emission will drive the final stage of the merger, but other dynamical processes must bring the SMBH into sufficient proximity for it to become effective. However, the obvious mechanisms which could contribute to this appear to stall before gravitational wave emission becomes significant, creating the “final parsec problem” [6]. Separately, the spectrum inferred from pulsar observations has less power at very low frequencies than expected for a stochastic background sourced by SMBH mergers. Both puzzles would be resolved if there is an additional source of drag at the centres of galaxies, which remains active as SMBH binaries reach the PTA band, ensuring prompt mergers while removing energy which would otherwise source gravitational radiation.

This paper explores Ultralight Dark Matter (ULDM) as a source of extra dynamical friction. ULDM is a dark matter candidate which consists of extremely light scalar particles [7–14], motivated by the possible existence of very light states in string theory [15]. Astrophysically, it can resolve apparent discrepancies between predictions of minimal Cold Dark Matter (CDM) and observations at subgalactic scales. Conversely, it matches the successful predictions of CDM at large scales.

A key feature of ULDM is the presence of solitonic cores at the centres of dark matter halos [16, 17]. Their central density can be much higher than in a comparable CDM halo, significantly increasing the dynamical friction experienced by SMBH binaries. Hui *et al.* [18] extended Chandrasekhar’s classic treatment of dynamical friction [19] to approximate the drag on a moving black hole in a uniform ULDM background. Inside a soliton, the situation is more complicated as the soliton responds coherently to the perturbation induced by the moving black hole. However, the dynamics of this system have been explored numerically for both single [20–23] and binary [24–26] black holes.

In particular, Ref. [26] showed that in large halos with ULDM masses of $\sim 10^{-21}$ eV the dynamical friction from the soliton would be significant at separations well below a parsec. In these simulations, the soliton is “pinched” by the SMBH, boosting the density and thus increasing the drag. In what follows, we develop a semi-analytic model of the dynamical friction on SMBH binaries at small separations. This includes the pinching and also allows for the possibility that ULDM does not provide all of the dark matter. This allows us to generate a library of gravitational strain spectra for different parameter combinations. Comparing this to the spectrum derived from the 15-year NANOGrav dataset, we can constrain the ULDM particle mass and fraction.

This paper builds on previous studies of the impact of ULDM on the gravitational wave background from SMBH binaries. In particular, Aghaie *et al.* [27] impose constraints on the soliton and particle mass under the assumption that the dark matter consists entirely of ULDM and that the SMBHs are larger than the solitons. We generate a synthetic spectrum and also allow for mixed ULDM and CDM models, but their findings are consistent with ours. Separately, two of us (ST and CG) looked at the related issue of drag on SMBH binaries in self-interacting dark matter [28], and this analysis

* shreyas.tiruvaskar@pg.canterbury.ac.nz

† russell.boey@auckland.ac.nz

‡ r.easther@auckland.ac.nz

§ chris.gordon@canterbury.ac.nz

builds on tools developed for that work.

We find that for a particle of around 10^{-21} eV the drag is sufficient to solve the final parsec problem and to reduce the long wavelength power in the stochastic gravitational wave background, such that the 68% credible interval of $\log_{10}(m/10^{-22}\text{eV}) = 0.84^{+0.44}_{-0.48}$. Interestingly, the drag remains effective if the mass of the central soliton is reduced, as would happen with a mixture of ULDM and regular CDM. As a result, our constraints are largely independent of the assumed ULDM fraction.

This apparent paradox arises because the stochastic gravitational wave background is primarily sourced by large black holes merging in the most massive halos. In these systems, the mass of the SMBH binary is expected to be similar to the soliton mass, given the usual ULDM core-halo relationship [17]. This increases the impact of pinching with a fractional ULDM component, counteracting the lower soliton mass, which, together with changes to the set of halos which undergo mergers, largely offsets variations in the ULDM fraction. Consequently, while the full range of ULDM particle masses is potentially excluded in a ULDM-only universe [29], much of the parameter range in which the drag improves the fit to PTA data is consistent with all other observations.

That said, the improved fit to observations comes with several caveats. In particular, our drag model should be viewed as a well-informed hypothesis, rather than a rigorous model. In particular, SMBH mergers occur in the wake of the merger of their parent galaxies and their central solitons. The resulting soliton will be highly excited, but even the best ULDM-SMBH drag simulations begin with an unperturbed soliton [23]. Secondly, there have been no detailed studies of the soliton properties in fractional ULDM models, beyond Ref. [30], which uses a fixed single particle mass and halo mass but varies the mass fraction. Thirdly, the relevant scaling relations suggest that SMBH and soliton masses are similar in the systems which contribute to the stochastic background, but the core-halo relation does not account for the presence of SMBH. That said, these assumptions point to productive lines of inquiry for future studies of ULDM dynamics.

Separately, the literature is rich with ‘‘anomalies’’ that resolved themselves as more data was obtained and analytic tools improved. Studies of the low-frequency stochastic gravitational wave background are in their infancy, and this analysis cannot ‘‘discover’’ ULDM with any more confidence than that with which the low-frequency deficit in the stochastic gravitational wave background has been detected. That said, if the low-frequency deficit is not confirmed by future analyses, the approach developed here could rule out a significant fraction of the currently permitted ULDM parameter space.

The structure of this paper is as follows. Section II introduces the Schrödinger-Poisson equations, the semi-analytic model and the computation of the orbital decay rate from these profiles. Section III describes the calculation of the gravitational strain spectrum, and Section IV discusses the parameter estimation. We discuss our re-

sults in Section V and conclude in Section VI.

II. SMBH-ULDM DYNAMICS

A. Schrödinger-Poisson System

In the non-relativistic regime, ULDM is governed by the Schrödinger-Poisson equations, or

$$i\hbar\dot{\psi} = -\frac{\hbar^2}{2m}\nabla^2\psi + m(\Phi_U + V)\psi, \quad (1)$$

and

$$\nabla^2\Phi_U = 4\pi Gm|\psi|^2. \quad (2)$$

Here ψ is the ULDM field, m is the ULDM particle mass, Φ_U is the ULDM gravitational potential, and V is that external gravitational potential sourced by the black hole binary. In mixed dark matter scenarios, we neglect the potential of the CDM halo as its scale radius is considerably larger than the soliton for most dark matter fractions we consider. As such, the potential is essentially constant and has no impact on the soliton profile.

ULDM solitons are ground state solutions to the Schrödinger-Poisson equations. Following Ref [23] we consider only the impact of the soliton itself on drag, neglecting the impact of the outer halo. At separations relevant to the PTA frequency range, we would not expect any interactions between the binary and the halo outside of the soliton [31]. However, this does neglect the impact of interactions between the halo and the soliton, which induce a random walk on the soliton [32, 33] and may affect the binary dynamics.

B. Orbital Decay Rate

For a given black hole mass, we use the relationships found in Ref. [34] (hereafter referred to as Agazie2023) to determine the corresponding stellar mass,

$$\log_{10}\left(\frac{M_{\text{BH}}}{M_{\odot}}\right) = \mu + \alpha_{\mu}\log_{10}\left(\frac{M_{\text{bulge}}}{10^{11}M_{\odot}}\right) + \mathcal{N}(0, \epsilon_{\mu}), \quad (3)$$

where μ , α_{μ} , and ϵ_{μ} parameterise the relationship between the black hole mass (M_{BH}) and the bulge mass (M_{bulge}). Here, we set α_{μ} to 1.1 following the fiducial value given in Table 2 of Agazie2023 while μ varies in our analysis. The Gaussian random scatter is denoted by $\mathcal{N}(0, \epsilon_{\mu})$; it has zero mean and its standard deviation ϵ_{μ} is also varied, as discussed in Section IV. The fraction of the galaxy’s stellar mass present in the stellar bulge is M_{bulge} , and it is related to the overall stellar mass of the galaxy M_{\star} by

$$M_{\text{bulge}} = 0.615 \cdot M_{\star}. \quad (4)$$

The stellar mass is, in turn, used to find the halo mass, M_h , through the relationship [35],

$$\frac{M_\star}{M_h}(z) = 2A(z) \left[\left(\frac{M_h}{M_A(z)} \right)^{-\beta(z)} + \left(\frac{M_h}{M_A(z)} \right)^{\gamma(z)} \right]^{-1}, \quad (5)$$

where z is the redshift, and we use the parameters from Table 3 of Ref. [35] and solve for M_h numerically. Given a UDLM particle mass m , we find the soliton mass from the canonical core-halo mass relationship [17],

$$M_c = \frac{1}{4a^{1/2}} \left(\frac{\zeta(z)}{\zeta_0(z)} \right)^{1/6} \left(\frac{M_{\text{ULDM}}}{M_{\text{min},0}} \right)^{1/3}, \quad (6)$$

$$\zeta(z) = \frac{18\pi^2 + 82(\Omega_m(z) - 1) - 39(\Omega_m(z) - 1)^2}{\Omega_m(z)} \quad (7)$$

and

$$M_{\text{min},0} = \frac{32\pi\zeta(0)^{1/4}}{375^{1/4}(H_0 m/\hbar)^{3/2}\Omega_{m0}^{3/4}} \rho_{m0}, \quad (8)$$

where a is the scale factor and H_0 is the present value of Hubble's constant.

We defined $M_{\text{ULDM}} = fM_h$ to accommodate models in which ULDM contributes only some of the dark matter. Naively, f represents the ULDM fraction, or

$$f = \frac{\Omega_{\text{ULDM}}}{\Omega_{\text{ULDM}} + \Omega_{\text{CDM}}} \times \frac{\Omega_{\text{DM}}}{\Omega_{\text{M}}}. \quad (9)$$

There is significant ambiguity in the core-halo relation itself [17, 36–44] and it has not been investigated for mixed models. However, it is unlikely that the soliton mass will scale linearly with the ULDM fraction. On top of this, analyses of the core-halo relationship have neglected the baryonic component of the universe, although it is included in equation (9). In practice, f thus expresses the relationship between the expected and actual soliton masses and not the actual ULDM fraction.

In simulations of halo collapse in mixed models [30] with $m = 2.5 \times 10^{-22} \text{eV}$ and halo masses of $\mathcal{O}(10^9)M_\odot$ solitons do not form if $f \lesssim 0.3$. In the very largest halos (which are our primary interest), the central soliton will be particularly compact, and the lower bound on f will presumably be smaller. We take $f \geq 0.01$ in what follows,

which is a somewhat arbitrary bound but our results do not depend on its specific value. Note too that the definition of f in Ref. [30] does not have the factor of $\Omega_{\text{DM}}/\Omega_{\text{M}}$ as baryons are not included in that analysis.

Unperturbed ULDM solitons have a universal profile, which is the ground state of the Schrödinger-Poisson system and is approximated by [16]

$$\rho(r) = \frac{1.9(m/10^{-23} \text{eV})^{-2}(r_c/\text{kpc})^{-4}}{(1 + 0.091(r/r_c)^2)^8} M_\odot \text{pc}^{-3}. \quad (10)$$

The core radius r_c is the point at which the density is 50% of the central density, and the mass contained within it is $M_c = 0.2408M_s$, where M_s is the total soliton mass. The usual scaling relations suggest that the ratio of the masses of the black hole and the soliton is largest in the most massive halos, which contribute most of the stochastic signal. However, since it is not known how the core-halo mass relation responds to the presence of the SMBH, we simply take the unmodified form.

We compute dD/dt (where D is the distance between the SMBH) by extending the approach of Ref. [26]. The expected drag is [18],

$$F_i = \frac{4\pi G^2 M_i^2 \rho_i}{v_i^2} C_i, \quad (11)$$

where subscript i indicates values associated with one of the black holes. The coefficient of friction C_i is

$$C_i = \text{Cin}(2k_i \tilde{r}_i) + \frac{\sin(2k_i \tilde{r}_i)}{2k_i \tilde{r}_i} - 1 + \dots \quad (12)$$

where $\text{Cin}(x) = \int_0^x (1 - \cos t)/t dt$, $r_i = |\mathbf{r}_i|$, $k_i = mv_i/\hbar$, \tilde{r}_i is a cutoff taken to be $\tilde{r}_i = \alpha r_i$ and α is a numerical parameter less than unity [25]. We fix $\alpha = 0.4$, based on the simulations in Ref. [26].

We assume the centre of mass of the binary and the soliton are both at the origin, giving $M_1 \mathbf{r}_1 + M_2 \mathbf{r}_2 = 0$. The velocities of the black holes are thus

$$v_i = \sqrt{\frac{GM_{\text{enc}i}}{r_i} + \frac{GM_j^3}{(M_i + M_j)^2 r_i}}, \quad (13)$$

where subscript j indicates the other black hole. This provides the torque,

$$\begin{aligned} \frac{dL_i}{dt} &= \frac{dr_i}{dt} \frac{dL_i}{dr_i} \\ &= \frac{dr_i}{dt} \frac{M_i \sqrt{G}}{2} \times \left(\sqrt{\frac{M_{\text{enc}i} + \frac{M_j^3}{(M_i + M_j)^2}}{r_i}} + \frac{dM_{\text{enc}i}}{dr_i} \sqrt{\frac{r_i}{M_{\text{enc}i} + \frac{M_j^3}{(M_i + M_j)^2}}} \right) \end{aligned}$$

$$= \frac{dr_i}{dt} \frac{M_i}{2} \left(v_i + \frac{4\pi r_i^2 \rho_i G}{v_i} \right), \quad (14)$$

where in the final line we have made use of spherical symmetry to find dM_{enc_i}/dr_i . This can be equated to the torque due to dynamical friction, $-F_i r_i$, to find dr_i/dt ,

$$\frac{dr_i}{dt} = -\frac{8\pi G^2 M_i \rho_i}{v_i^3 + 4\pi r_i^2 \rho_i G v_i} C r_i. \quad (15)$$

Summing these two terms gives dD/dt .

The density in equation (15) depends on the soliton profile, which is “pinched” by the pair of SMBH. We estimate the modified profile by assuming that the total mass of the binary is located at the soliton centre. We additionally assume time-independence (in the radial direction) with the ansatz $\psi(\mathbf{r}, t) = e^{i\beta t} F(r)$ and $\Phi_U(\mathbf{r}, t) = \phi(r)$ and the resulting Schrödinger-Poisson equation is

$$F''(r) + \frac{2}{r} F'(r) - 2\tilde{\phi}(r)F(r) + 2\frac{M_{BH}}{r} F(r) = 0, \quad (16)$$

$$\tilde{\phi}''(r) - 4\pi F^2(r) + \frac{2}{r} \tilde{\phi}'(r) = 0, \quad (17)$$

where $\tilde{\phi}(r) = \phi(r) + \beta$ and $F'(r) = dF/dr$. The equation is solved via the shooting method, with $F(0) = 1$, $F'(0) = \tilde{\phi}'(0) = 0$, and $F(r_{\text{max}}) = \phi(r_{\text{max}}) = 0$, where r_{max} is a cut-off radius where the soliton profile is negligible. The mass of the soliton can then be found by integrating the profile, and this in turn gives the mass ratio between the black hole and the soliton.

If $e^{i\beta t} F(r)$ solves the radial Schrödinger-Poisson equations, the scaled profile $e^{i\gamma\beta t} \gamma F(\sqrt{\gamma}r)$ is also a solution. After restoring dimensionality, γ is fixed by requiring the integrated mass (recalling that the density is proportional to $|\psi|^2$) matches the desired soliton mass, and the black hole to soliton mass ratio is invariant with γ . By varying the black hole mass, we can solve iteratively for the profile¹ and, as noted earlier, the pinching is significant when the black hole mass approaches or exceeds the soliton mass.

We tested these profiles by simulating binaries in circular orbits inside soliton profiles with AXIONYX [30], using the approach of Ref. [26]. There is good overlap for tight binaries, but, unsurprisingly, if the binary is outside the core radius of the pinched soliton, this approach breaks down. Figure 1 shows the central density and representative radial profiles for examples when the total SMBH mass is $10M_s$. Given the pinched density profile, we can compute dD/dt at any separation.

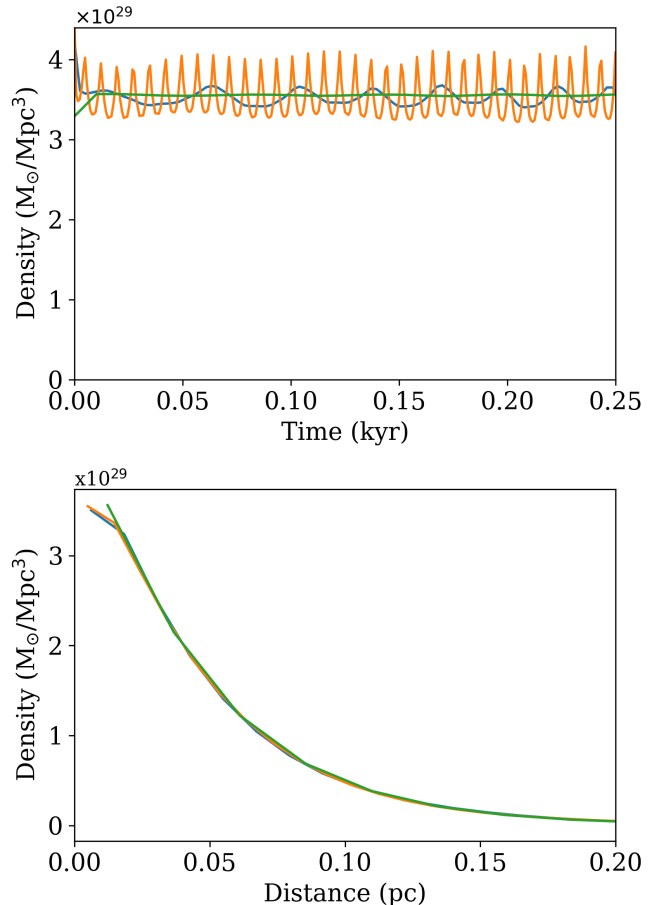


FIG. 1: (Top) Central densities as a function of time for an equal mass binary (blue), a binary with mass ratio 1 : 3 (orange), and a stationary central black hole (green); the total SMBH mass is $10M_s$. For the equal mass case, the initial radius is 0.015pc; the unequal mass case has 0.03pc and 0.01pc; $r_c \approx 0.0296$ pc. The central densities of the binaries oscillate but are near the single black hole value. (Bottom) Radial density profiles at $t \sim 0.264$ kyr.

C. Simple Model

To assess the sensitivity of the results to our model for the dynamical friction, we also consider a simplified model, without pinching, developed by Koo *et al.* [25] and extended in Ref. [26]. The unpinched soliton profile is given by equation (10). In this case, the SMBH separations are much smaller than r_c when gravitational

¹In practice, we generated profiles for mass ratios between 0 and 82.15 and interpolated between them.

wave emission occurs, so the black hole velocities are

$$v_i = \sqrt{\frac{GM_j^3}{(M_i + M_j)^2 r_i}}. \quad (18)$$

since we can neglect the ULDM enclosed by their orbit.

The expression for C_i also simplifies when $k_i \tilde{r}_i \ll 1$, and a Taylor expansion provides $C_i = (k_i \tilde{r}_i)^2 / 3$. Finally, the ULDM density near the black holes is close to the central density, so we set $\rho_1 = \rho_2 = \rho(0)$. For this case

$$\frac{dr_i}{dt} = \frac{8\pi G^{3/2} M_i (1 + M_i/M_j) \rho(0) \alpha^2 m^2 r_i^{3.5}}{3\hbar^2 \sqrt{M_j}}, \quad (19)$$

and we again find dD/dt by summing these two contributions.

D. Scaling expectations

In both models dD/dt depends much more strongly on the ULDM particle mass m than on f . Via the standard scaling relations [17] the simple model has $r_c \propto m^{-1} f^{-1/3}$, $\rho(0) \propto m^{-2} r_c^{-4}$, and $dD/dt \propto \rho(0) m^2$. As such,

$$\frac{dD}{dt} \propto m^4 f^{4/3}. \quad (20)$$

The scaling relationships in the realistic model are not as clean, and in that case, the effect is counter-intuitively enhanced by the soliton mass decreasing as m increases, since $M_c \propto m^{-1}$. This increases the pinching for a fixed black holes mass (and thus fixed halo mass, given our other assumptions), boosting the central density and dD/dt relative to the simple model. Conversely, increasing f increases the soliton mass, which decreases the pinching (since $M_c \propto f^{1/3}$), so the density scales more slowly than in the simple model. The outcome is that dD/dt and the decay timescale are much more sensitive to m than to f for both models. This will be reflected in our results, which allow a wide range of f but pick out a narrower range of m , particularly with the realistic model.

III. GRAVITATIONAL STRAIN SPECTRUM

The gravitational strain of a single binary source is given in equation (6) of Agazie2023 as

$$h_s^2(f_{\text{gw}}) = \frac{32}{5c^8} \frac{(GM)^{10/3}}{d_c^2} (2\pi f_{\text{orb}})^{4/3}, \quad (21)$$

where d_c is the comoving distance to the source, which is a function of redshift z . The binary chirp mass is denoted by \mathcal{M} , f_{gw} is the observer-frame gravitational wave frequency, and f_{orb} is the source-frame orbital frequency of the binary. The source frame gravitational

wave frequency is double the binary orbital frequency, $f_{\text{gw-source}} = 2f_{\text{orb}}$. If the source is at redshift z , these frequencies are related by

$$f_{\text{gw}} = \frac{f_{\text{gw-source}}}{(1+z)} = \frac{2f_{\text{orb}}}{(1+z)}. \quad (22)$$

The chirp mass of the binary is given by equation (1) of Agazie2023,

$$\mathcal{M} = \frac{Mq^{3/5}}{(1+q)^{6/5}}, \quad (23)$$

where q is the mass ratio defined as M_2/M_1 with M_1 being the primary (heavier) black hole mass and M_2 being the secondary (lighter) black hole mass, and the total mass of the binary is ($M = M_1 + M_2$).

The total gravitational strain can be obtained by adding the individual binary strains using equation (5) of Agazie2023,

$$h_c^2(f_{\text{gw}}) = \int dM dq dz \frac{\partial^4 N}{\partial M \partial q \partial z \partial \ln f_{\text{orb}}} h_s^2(f_{\text{orb}}), \quad (24)$$

where $h_c(f_{\text{gw}})$ is the total characteristic strain of the GWB over a logarithmic frequency interval. Following equation (7) of Agazie2023, we write

$$\frac{\partial^4 N}{\partial M \partial q \partial z \partial \ln f_{\text{orb}}} = \frac{\partial^3 \eta}{\partial M \partial q \partial z} \cdot \tau(f_{\text{orb}}) \cdot 4\pi c (1+z) d_c^2 \quad (25)$$

where c is the speed of light. The differential volumetric number density of binaries is $\partial^3 \eta / \partial M \partial q \partial z$ and depends on (M, q, z) . It gives the number of binaries of mass M , mass ratio q , and redshift z that would be present in a unit volume and is calculated below.

The binary hardening timescale is the time (measured in the source frame, i.e. the centre of mass rest-frame of the SMBH binary) spent in a given logarithmic frequency interval is denoted $\tau(f_{\text{orb}})$. Following equations (44-48) from [28], $\tau(f_{\text{orb}})$ can be written as

$$\tau(f_{\text{orb}}) \equiv \frac{f_{\text{orb}}}{\dot{f}_{\text{orb}}} = -\frac{3}{2} \frac{D}{\dot{D}}. \quad (26)$$

The total characteristic strain is then

$$h_c^2(f_{\text{gw}}) = \int dM dq dz \frac{\partial^3 \eta}{\partial M \partial q \partial z} \cdot \left(-\frac{3}{2} \frac{D}{\dot{D}} \right) \times 4\pi c (1+z) d_c^2 \times \frac{32}{5c^8} \frac{(GM)^{10/3}}{d_c^2} (2\pi f_{\text{orb}})^{4/3}. \quad (27)$$

For the full model \dot{D} is given by equation (15) and by equation (19) for the simple model – given the dr_i/dt we add them to get \dot{D} .

Binary separation D is related to the observed gravitational wave frequency f_{gw} , total binary mass M , and

redshift z through equations (36) and (22). For each combination of (M, q, z) we evolve our binary system in 300 steps using \dot{D} , starting from a separation of $D = 1\text{pc}$, down to $D = \text{ISCO}$, where the ISCO is the innermost stable circular orbit, given by $6GM/c^2$. At each step of the evolution we have a specific value of D which gives us the corresponding f_{orb} , f_{gw} , and the source strain $h_s^2(f_{\text{orb}})$. This allows us to numerically evaluate the integral in equation (24) for each PTA frequency bin. Following Agazie2023, we set the integration limits to $M : (10^4 M_\odot, 10^{12} M_\odot)$, $q : (0.001, 1)$, and $z : (0.001, 10)$. We also require that contributions to the total strain are from binaries that merge within the age of the universe, ensuring that we only consider systems for which the final parsec problem is actually solved in our model.

We follow equation (22) from Agazie2023 to calculate the differential volumetric number density of the binaries,

$$\frac{\partial^3 \eta}{\partial M \partial q \partial z} = \frac{\partial^3 \eta_{\text{gal-gal}}}{\partial M_{\star 1} \partial q_{\star} \partial z} \frac{\partial M_{\star 1}}{\partial M} \frac{\partial q_{\star}}{\partial q}, \quad (28)$$

where $M_{\star 1}$ is the stellar mass of the primary merging galaxy and q_{\star} is the stellar mass ratio of the secondary to the primary galaxy. The relation between $M_{\star 1}$ and M_1 can be evaluated from equations (3) and (4), with we set α_μ to 1.1. Using these relations $\partial M_{\star 1} / \partial M$ and $\partial q_{\star 1} / \partial q$ are [28]

$$\begin{aligned} \frac{\partial M_{\star 1}}{\partial M} &= \frac{1}{\alpha_\mu} \frac{M_{\star 1}}{M} \\ \frac{\partial q_{\star}}{\partial q} &= \frac{1}{\alpha_\mu} q_{\star}^{1-\alpha_\mu}. \end{aligned} \quad (29)$$

and $M_{\star 1}$ and q_{\star} can be written in terms of M_1 and M_2 , which in turn can be expressed in terms of M and q .

For $\partial^3 \eta_{\text{gal-gal}} / \partial M_{\star 1} \partial q_{\star} \partial z$, we refer to equation (13) from Agazie2023,

$$\frac{\partial^3 \eta_{\text{gal-gal}}}{\partial M_{\star 1} \partial q_{\star} \partial z} = \frac{\Psi(M_{\star 1}, z')}{M_{\star 1} \ln(10)} \cdot \frac{P(M_{\star 1}, q_{\star}, z')}{T_{\text{gal-gal}}(M_{\star 1}, q_{\star}, z')} \cdot \frac{\partial t}{\partial z'}. \quad (30)$$

Here, z' is the redshift at the time before the galaxy merger starts. Everything in the RHS is calculated at this pre-merger redshift z' . The redshift in the LHS is the redshift after the merger is complete, i.e., $z' = z'[t]$ and $z = z[t + T_{\text{gal-gal}}]$.

To calculate $\Psi(M_{\star 1}, z')$, $P(M_{\star 1}, q_{\star}, z')$, and $T_{\text{gal-gal}}(M_{\star 1}, q_{\star}, z')$, we use equation (15), equation (16), equation (19), and equation (20) from Agazie2023:

$$\Psi(M_{\star 1}, z') = \ln(10) \Psi_0 \left[\frac{M_{\star 1}}{M_\psi} \right]^{\alpha_\psi} \exp\left(-\frac{M_{\star 1}}{M_\psi}\right) \quad (31)$$

where

$$\begin{aligned} \log_{10}(\Psi_0 / \text{Mpc}^{-3}) &= \psi_0 + \psi_z \cdot z', \\ \log_{10}(M_\psi / M_\odot) &= m_{\psi,0} + m_{\psi,z} \cdot z', \\ \alpha_\psi &= 1 + \alpha_{\psi,0} + \alpha_{\psi,z} \cdot z'. \end{aligned} \quad (32)$$

The values and prior ranges of all these parameters are given in Table I.

The galaxy pair fraction $P(M_{\star 1}, q_{\star}, z')$ and the galaxy merger time $T_{\text{gal-gal}}(M_{\star 1}, q_{\star}, z')$ are calculated using equations (19) and (20) of Agazie2023. We follow their analysis and use the same values for the parameters of the galaxy pair fraction and merger time, which can be found in Table B1 of Agazie2023.

Symbol	Fiducial Value	Priors
$\log_{10}(m_{22})$	–	$\mathcal{U}(-2.5, 2.5)$
$\log_{10}(f)$	–	$\mathcal{U}(-2, 0)$
ψ_0	–	$\mathcal{N}(-2.56, 0.4)$
ψ_z	–0.60	–
$m_{\psi,0}$	–	$\mathcal{N}(10.9, 0.4)$
$m_{\psi,z}$	+0.11	–
$\alpha_{\psi,0}$	–1.21	–
$\alpha_{\psi,z}$	–0.03	–
μ	–	$\mathcal{N}(8.6, 0.2)$
α_μ	+1.10	–
ϵ_μ	–	$\mathcal{N}(0.32, 0.15)$ dex
$f_{\star, \text{bulge}}$	+0.615	–

TABLE I: Priors and fiducial values for the model parameters

The last term in the RHS of equation (30) is $dt/\partial z'$, can be calculated using the redshift-time relation

$$\frac{dt}{dz'} = \frac{1}{(1+z')H(z')}. \quad (33)$$

where

$$H(z) = H_0 \sqrt{\Omega_m (1+z)^3 + \Omega_\Lambda}. \quad (34)$$

and Ω_Λ is the dark energy fraction. Following NANOGrav (see Agazie2023) we use the WMAP9 values for H_0 , Ω_m , and Ω_Λ , $H_0 = 69.33 \text{ km s}^{-1} \text{ Mpc}^{-1}$, $\Omega_m = 0.288$ and $\Omega_\Lambda = 0.712$ [45].

While $\partial^3 \eta / \partial M \partial q \partial z$ can be calculated using the pre-merger redshift z' we need the post-merger redshift z for the other terms in the integral in equation (27). This is found from the pre-merger redshift z' and the galaxy merger time $T_{\text{gal-gal}}$ by numerically solving for $z_{\text{post-merger}}$ via

$$T_{\text{gal-gal}} = \int_t^{t+T_{\text{gal-gal}}} dt = \int_{z_{\text{post-merger}}}^{z_{\text{pre-merger}}} (1+z)H(z) dz. \quad (35)$$

With this, we are now fully equipped to calculate the characteristic strain spectrum $h_c(f)$.

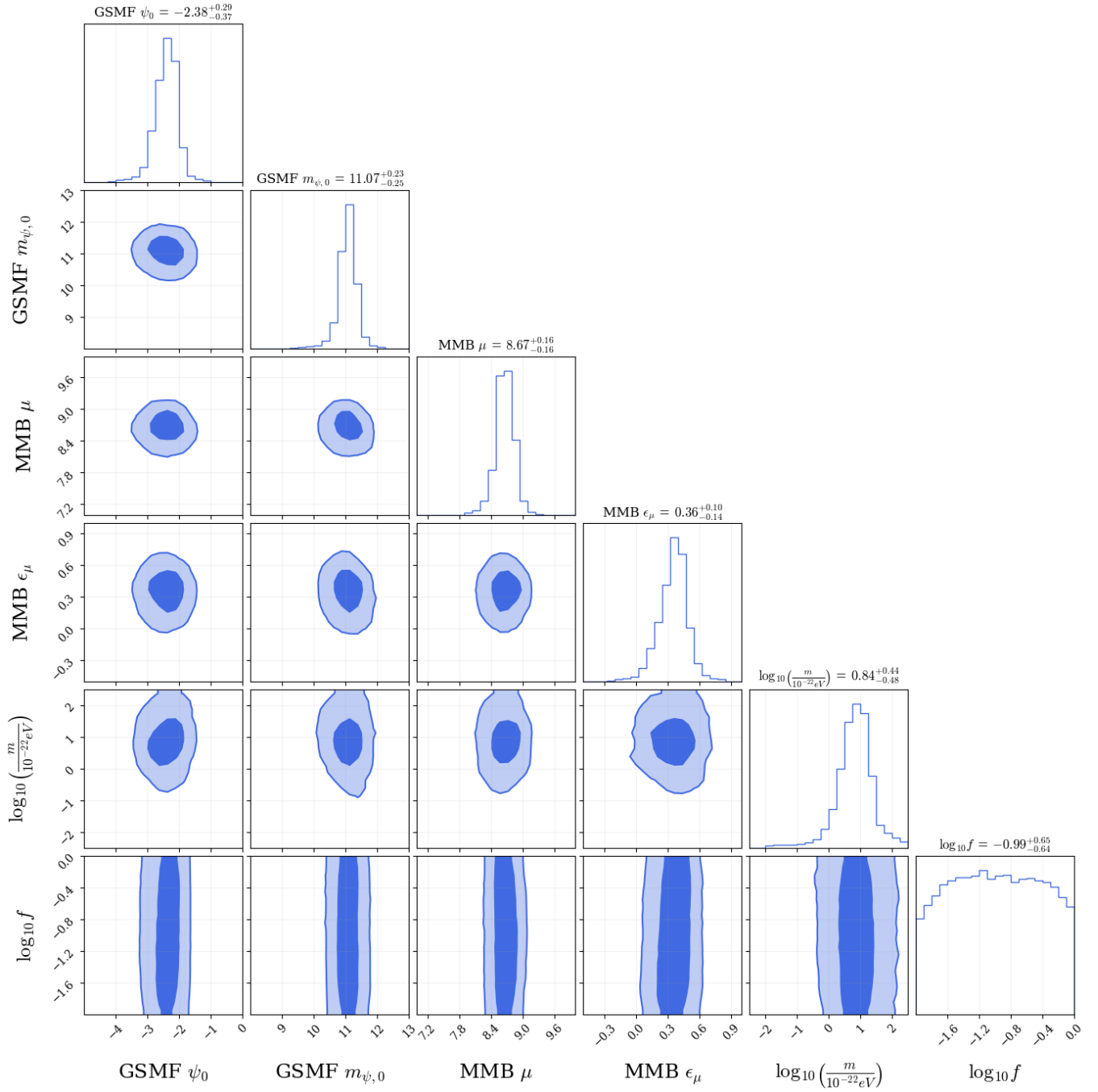


FIG. 2: Posterior distribution of model parameters with 68% and 95% confidence interval contours for the realistic model. Reported values correspond to the medians and their 68% credible intervals.

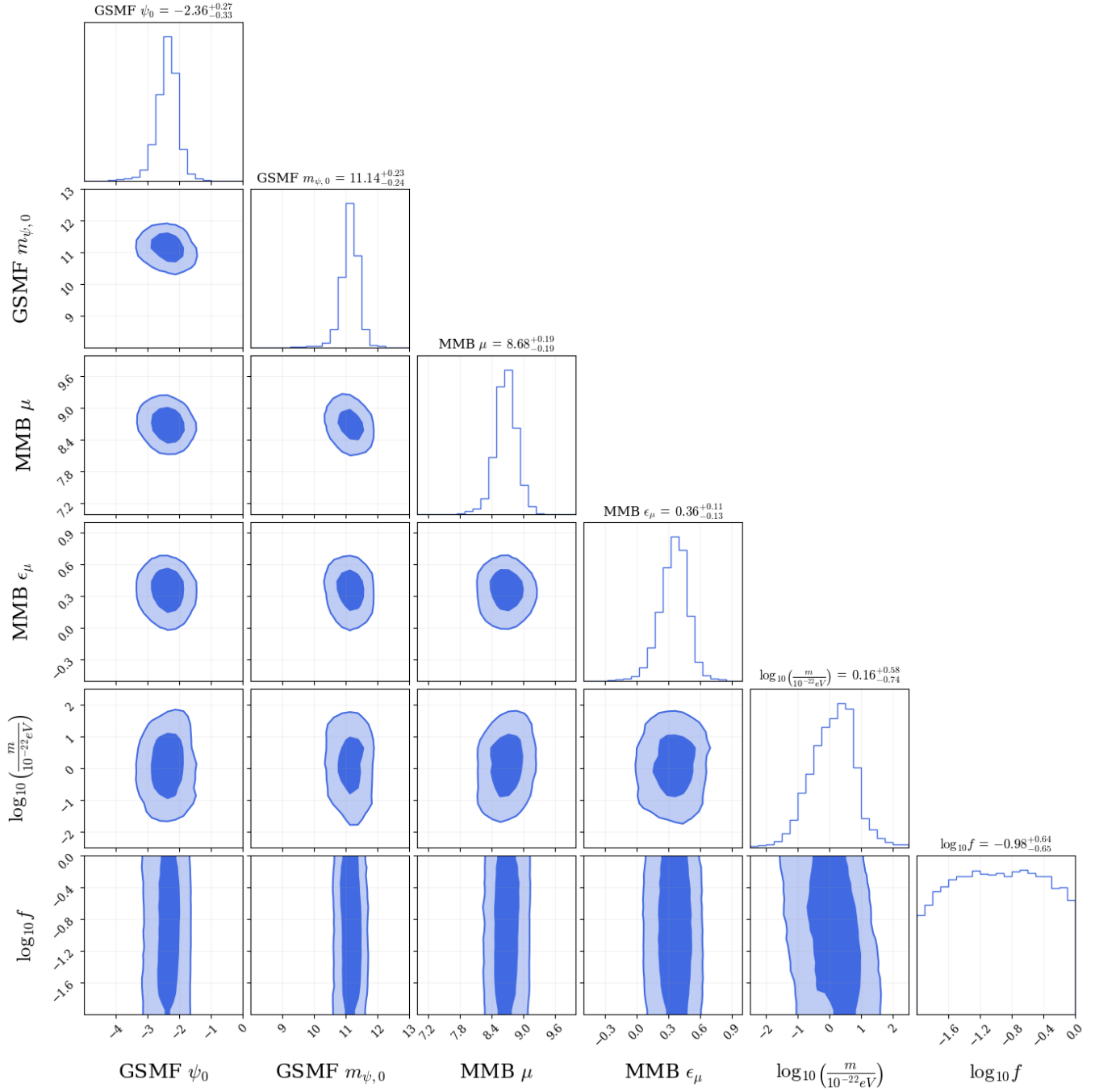


FIG. 3: Posterior distribution for the simple model; other settings match those of Figure 2.

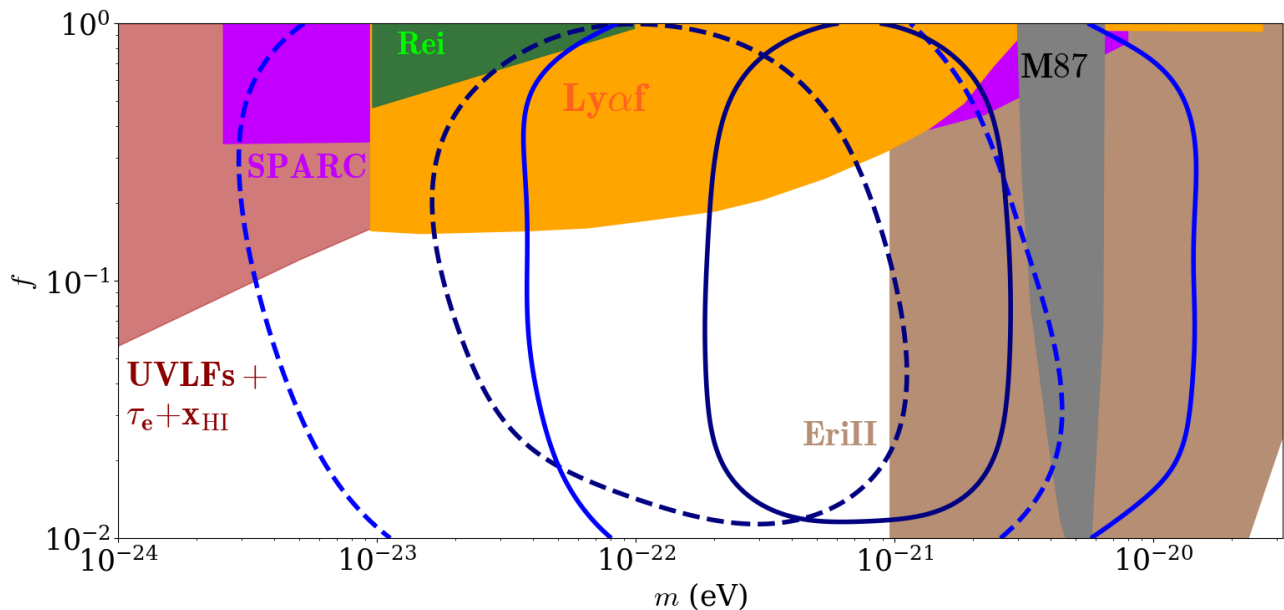


FIG. 4: The joint posterior for the ULDM particle mass and fraction is shown alongside existing constraints, as summarized in Ref. [29]. Dark blue and blue lines show 68 and 95% confidence intervals, respectively; the realistic and simple models are shown with solid and dashed lines, respectively.

IV. PARAMETER ESTIMATION

Our ULDM models, both simple and realistic, have six free parameters. The ULDM specific parameters are the particle mass m , which we express as $m/10^{-22}\text{eV} \equiv m_{22}$ and the ULDM fraction, defined in Section II B. The other parameters are contained within the galaxy stellar mass function (GSMF) $\Psi(M_*, z')$; ψ_0 and $m_{\psi,0}$ from equation (32), and the relation between M_{BH} and M_{bulge} (MMB), expressed in equation (3); μ and ϵ_μ , following Agazie2023. The priors are listed in Table I.

We generate a library of gravitational strain spectra for SMBH binary mergers occurring within ULDM halos with different parameter combinations. We created 2000 unique combinations of the 6 model parameters following their prior distributions and ranges using Latin hypercube sampling. We generated 2000 realizations of strain spectra for each of the 2000 parameter combinations, as detailed in Section V-C of Ref. [28] and Section 3.2.2 of Agazie2023.

We then train a Gaussian process (GP) on the library, allowing us to interpolate strain values at any intermediate point in the parameter space, speeding up MCMC generation. We train one GP for the median values of the strain and another for the standard deviation. The GP predictions and calculated strains differ by less than $2\text{-}\sigma$, confirming that the sample size is sufficient.

The third and final step is MCMC creation. We used the NANOGrav 15-year dataset with Hellings-Downs correlated free spectrum modelled simultaneously with additional MP (monopole-correlated), DP (dipole-correlated) red noise, and CURN (common uncorrelated

red noise). We only used the strain values from the five lowest frequency bins of this dataset, as these dominate the fit to PTA data. These strain values (or, more accurately, their distributions) are used to calculate likelihoods and thus posterior distributions from MCMC chains. We use `holodeck` with modifications for our ULDM models for library generation, Gaussian process interpolation, and MCMC chain generation.

V. RESULTS AND ANALYSIS

The posterior distributions for the “simple” and “realistic” models are presented in Figures 2 and 3. The 95% region for ψ_0 matches well with the results of Ref. [46] who found a best fit of $\psi_0 \sim -2.5$. Our results for $(\psi_0, m_{\psi,0}, \mu, \epsilon_\mu)$ are in agreement with the results from those in Figure 10 of Agazie2023, a phenomenological model with astrophysical priors and with Ref. [28] for the self-interacting dark matter model.

For the realistic model, the median value and 68% credible interval of the ULDM particle mass m is $6.98^{+12.2}_{-4.7} \times 10^{-22}$ eV. For the simple model the allowed range is $1.43^{+4.0}_{-1.2} \times 10^{-22}$ eV. Figure 4 presents the 68% and 95% confidence parameter regions of our models, along with constraints on the ULDM parameter space [29], and we see that these overlap with significant regions that are permitted by observations. For both models, the ULDM particle mass is well constrained, but the fraction is not, confirming the expectations of Section II D.

Figure 5 shows the best-fit gravitational strain spectra. The corresponding parameter values at the maxi-

Model	ψ_0	$m_{\psi,0}$	μ	ϵ_μ	$\log_{10}\left(\frac{m}{10^{-22}\text{eV}}\right)$	$\log_{10} f$
Simple	-2.16	11.70	8.91	0.39	1.40	-1.39
Realistic	-2.22	11.34	8.59	0.43	0.97	-0.31

TABLE II: Maximum log-posterior values for the simple and realistic models.

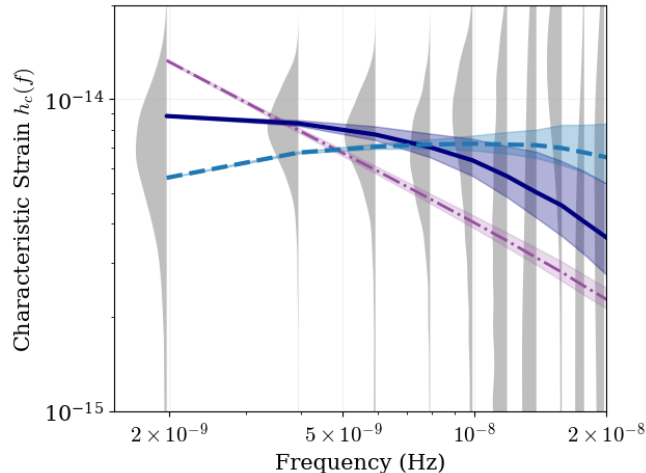


FIG. 5: The dark blue line corresponds to the best-fit spectra for the realistic ULDM model; the dashed blue line represents the simple model. The purple line is the gravitational wave-only model from Agazie2023. Grey violins are the 15-year NANOGrav data. Shaded regions around the lines highlight the 95% credible regions.

mum log-posterior are given in Table II.

Spectra for different values of $\log_{10}\left(\frac{m}{10^{-22}\text{eV}}\right)$ can be seen in Figures 6. We find that in the realistic model, the strain is more sensitive to changes in the particle mass than in the simplified model, as expected from our scaling expectations.

We check that the black holes are inside the core radius as they contribute to the PTA signal, to confirm the assumptions used to compute dD/dt . Recalling that f_{gw} is twice the orbital frequency, Kepler’s third law gives

$$D = \left(\frac{GM_{BH}}{\pi^2 f_{gw}^2} \right)^{\frac{1}{3}}, \quad (36)$$

where we have here neglected the piece of the soliton enclosed within the orbit.

Substituting $f_{gw\text{-source}} = 10^{-9}\text{Hz}$ gives the maximum relevant separation at which the binary radiates at PTA frequencies. Figure 7 compares this to r_c for SMBH binaries that primarily contribute to our signal in the realistic model, and all of them are inside r_c . In the simplified model, there is no pinching, and r_c is much larger than the orbital radius.

It would take a full numerical simulation to confirm that solitons form in the halos which host the largest

Model name	ELPD difference	DSE	ELPD diff./DSE
GW only	0	0	-
ULDM simple	0.14	3.00	0.05
ULDM realistic	1.91	3.14	0.61

TABLE III: LOO-CV model comparison

SMBH for a given ULDM fraction and particle mass, which is beyond the scope of this work. However, one consistency check is to compare the density of the naive soliton profile to that of the NFW profile of the cold dark matter component. We use the mass-concentration relationship in Ref [47] for the CDM component of the halo. If the soliton density is greater than the CDM density, it is more reasonable to assume soliton formation than otherwise.

Figure 8 makes this comparison for our maximum likelihood parameters and a halo with $10^8 M_\odot$ black holes, the mass range that makes the largest contribution to the PTA signal. The soliton density exceeds the NFW density when pinching is accounted for, although it may not be satisfied in the simple model. Both the soliton and NFW profiles are affected by changing halo masses at higher redshifts, but the soliton mass generally increases with redshift directly in the core-halo relation, while the NFW concentration plateaus, so this is expected to hold at higher redshifts.

Finally, we check the significance of the “signal” of ULDM in the PTA data via Bayesian “Leave one out cross-validation” (LOO-CV) model comparison [48–50]. This approach is computationally efficient as it needs only the already computed MCMC chains [49]. We compare the simple and realistic ULDM models to the default model, where only gravitational waves contribute to energy loss.

The “ELPD difference” represents the difference in expected log predictive density between each model and the best model, and “DSE” represents the standard error of the ELPD difference. If the ratio of ELPD difference is greater than 3 standard errors (or DSE), the models are considered to be significantly different. We use the Python package `ArviZ` [51] to find the results in Table III. In our case, these ratios are smaller than unity, so there is no meaningful “detection” even though the posteriors on the ULDM parameters are nontrivial. As noted in the Introduction, this is not surprising – the result is driven by the lowest frequency bin, and the statistical power of the deficit itself is not overwhelming.

VI. DISCUSSION AND CONCLUSION

We used the gravitational wave background detected in pulsar timing experiments to constrain the ULDM particle mass. To do this, we considered mergers of super-massive black holes in ULDM halos with solitonic cores, developing a semi-analytic model of the dynamical fric-

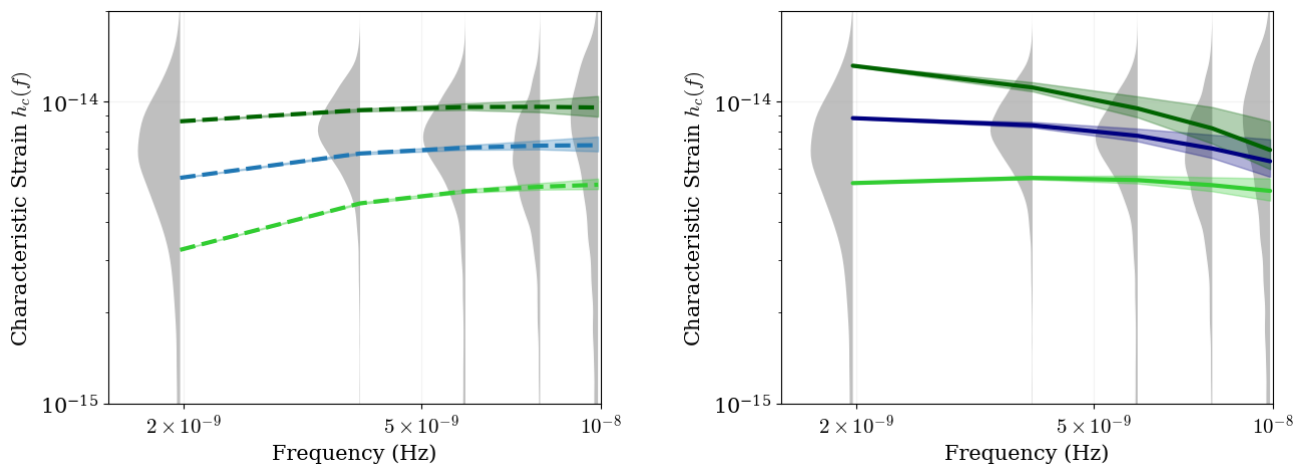


FIG. 6: Strain spectra for a range of particle masses in both the simple (left- dashed lines) and realistic (right- solid lines) models. Blue lines are the best-fit spectra. Dark green lines correspond to the spectra with best-fit $\log_{10} \left(\frac{m}{10^{-22} \text{eV}} \right) - 0.2$ and the light green to best-fit $\log_{10} \left(\frac{m}{10^{-22} \text{eV}} \right) + 0.2$.

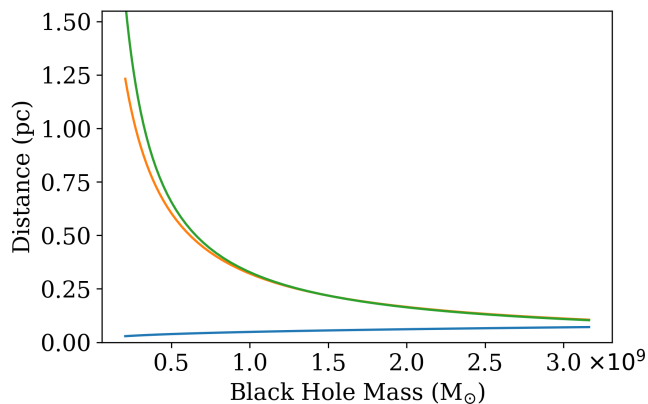


FIG. 7: Comparison of the soliton core radius at $z=10$ (orange) and $z=0$ (green) with the maximum separation of the binary where it emits in the PTA band (blue). This represents the maximum possible value that orbital radius can take for extreme binary mass ratios, which in practice do not produce large strain contributions.

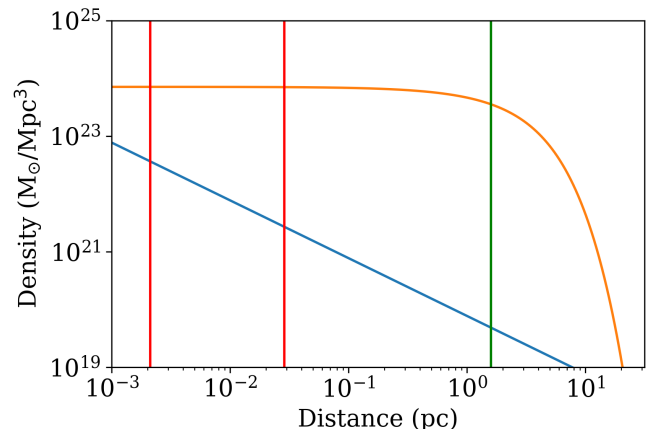


FIG. 8: Comparisons of the soliton (orange) and NFW profile (blue) densities for a galaxy corresponding to $M_{\text{BH}} = 2.06 \times 10^8 M_{\odot}$ at $z=0$. Red vertical lines correspond to the frequencies of the PTA band, while the green vertical line is the core radius of the soliton.

tion experienced by an SMBH binary inside a soliton.

We have confirmed that ULDM can contribute significantly to the orbital decay of SMBH binaries at the centres of the largest galaxies. The additional friction remains significant as binaries enter the pulsar timing band, resolving any “final parsec problem” and also suppressing the low-frequency component of the stochastic background, improving the fit to current data. Moreover, this shows that future pulsar timing measurements of the stochastic gravitational wave background will significantly constrain any ULDM contribution to the dark matter component of the universe.

This work is based on an improved semi-analytic model for the dynamical friction on an SMBH binary in a ULDM soliton. This includes a heuristic rescaling of the

soliton mass, accounting for both uncertainty in the core-halo relation and scenarios with a fractional ULDM dark matter contribution. Interestingly, scalings within the model yield the prediction that the dynamical friction from ULDM decreases slowly with the ULDM fraction. As a result, the contribution to binary decay remains significant even in scenarios with a relatively small fraction of ULDM.

Because we work directly with a galaxy merger history, we can identify the systems which make the largest contribution to the stochastic background; these are the halos in which the SMBH pair has roughly twice the mass of the soliton. This contrasts with previous work on ULDM-SMBH interactions by Aghaie *et al* [27], which only considers systems where the black hole mass is at least five

times larger than the soliton mass, but our results are consistent with and complementary to theirs.

Constraints on astrophysical parameters in our analyses are in excellent agreement with previous results [28, 34, 46]. Significant pieces of the ULDM parameter space are ruled out by a variety of astrophysical constraints. However, much of the region inside the joint posterior distribution for the ULDM parameters is consistent with all currently available constraints [29].

We developed two models of the dynamical friction – the “realistic” scenario accounts for SMBH binary pinching the soliton profile, whereas the “simple” one does not. The best-fit spectra for both models match the data with a similar level of quality. In both cases, scaling relations in the model mean that drag drops as a small, fractional power of the ULDM fraction. As a result, we cannot put a clear lower bound on the ULDM fraction. That said, the model relies on a number of hypotheses, and the soliton mass is set via the “standard” core-halo relation. Critically, this relation is an almost entirely unexplored relationship in models with a central SMBH, baryons and a mixture of ULDM and CDM. Each of these questions is an important avenue for future investigation. We have also assumed that there is a single ULDM component, which need not be the case, given that the arguments used to produce light scalar fields will typically be consistent with a spectrum with several such species [52].

Constraints on the stochastic background are expected to improve substantially as higher-quality PTA data becomes available in the next few years. If the data continues to suggest an absence of power at low frequencies

(relative to the naïve Hellings-Downs curve), it is likely that PTA observations will put tight constraints on the mass of any ULDM particle. Conversely, if this feature is not present in future datasets, PTA observations will put stringent constraints on the overall ULDM parameter space.

As noted above, the detailed drag models we use rely on several hypotheses. However, both the simple and “realistic” models remove power from the stochastic background at low frequencies, giving confidence in our conclusion that PTA data is sensitive to the presence of ULDM in galaxies is robust. However, specific constraints will require a more detailed understanding of ULDM-SMBH interactions in recently merged galaxies.

ACKNOWLEDGMENTS

We gratefully acknowledge support from the Marsden Fund Council grant MFP-UOA2131 from New Zealand Government funding, managed by the Royal Society Te Apārangi, and we acknowledge the use of New Zealand eScience Infrastructure (NeSI) high-performance computing facilities. We thank Laura Burn, Emily Kendall, Renate Meyer, Pierre Mourier and Frank Wang for helpful discussions. We are grateful to Hovav Lazare for providing the code used to generate the other constraint contours in Fig. 4 and to the authors of `holodeck` for making the package available.

-
- [1] G. Agazie *et al.* (NANOGrav), The NANOGrav 15 yr Data Set: Evidence for a Gravitational-wave Background, *Astrophys. J. Lett.* **951**, L8 (2023), [arXiv:2306.16213 \[astro-ph.HE\]](#).
 - [2] J. Antoniadis *et al.* (EPTA, InPTA:), The second data release from the European Pulsar Timing Array - III. Search for gravitational wave signals, *Astron. Astrophys.* **678**, A50 (2023), [arXiv:2306.16214 \[astro-ph.HE\]](#).
 - [3] H. Xu *et al.*, Searching for the Nano-Hertz Stochastic Gravitational Wave Background with the Chinese Pulsar Timing Array Data Release I, *Res. Astron. Astrophys.* **23**, 075024 (2023), [arXiv:2306.16216 \[astro-ph.HE\]](#).
 - [4] M. T. Miles *et al.*, The MeerKAT Pulsar Timing Array: the first search for gravitational waves with the MeerKAT radio telescope, *Mon. Not. Roy. Astron. Soc.* **536**, 1489 (2024), [arXiv:2412.01153 \[astro-ph.HE\]](#).
 - [5] D. J. Reardon *et al.*, Search for an Isotropic Gravitational-wave Background with the Parkes Pulsar Timing Array, *Astrophys. J. Lett.* **951**, L6 (2023), [arXiv:2306.16215 \[astro-ph.HE\]](#).
 - [6] M. Milosavljevic and D. Merritt, The Final parsec problem, *AIP Conf. Proc.* **686**, 201 (2003), [arXiv:astro-ph/0212270](#).
 - [7] J. Preskill, M. B. Wise, and F. Wilczek, Cosmology of the Invisible Axion, *Phys. Lett. B* **120**, 127 (1983).
 - [8] L. F. Abbott and P. Sikivie, A Cosmological Bound on the Invisible Axion, *Phys. Lett. B* **120**, 133 (1983).
 - [9] W. Hu, R. Barkana, and A. Gruzinov, Cold and fuzzy dark matter, *Phys. Rev. Lett.* **85**, 1158 (2000), [arXiv:astro-ph/0003365](#).
 - [10] J. Lesgourgues, A. Arbey, and P. Salati, A light scalar field at the origin of galaxy rotation curves, *New Astron. Rev.* **46**, 791 (2002).
 - [11] A. Suárez, V. H. Robles, and T. Matos, A Review on the Scalar Field/Bose-Einstein Condensate Dark Matter Model, *Astrophys. Space Sci. Proc.* **38**, 107 (2014), [arXiv:1302.0903 \[astro-ph.CO\]](#).
 - [12] P. W. Graham, I. G. Irastorza, S. K. Lamoreaux, A. Lindner, and K. A. van Bibber, Experimental Searches for the Axion and Axion-Like Particles, *Ann. Rev. Nucl. Part. Sci.* **65**, 485 (2015), [arXiv:1602.00039 \[hep-ex\]](#).
 - [13] D. J. E. Marsh, Axion Cosmology, *Phys. Rept.* **643**, 1 (2016), [arXiv:1510.07633 \[astro-ph.CO\]](#).
 - [14] E. G. M. Ferreira, Ultra-light dark matter, *Astron. Astrophys. Rev.* **29**, 7 (2021), [arXiv:2005.03254 \[astro-ph.CO\]](#).
 - [15] P. Svrcek and E. Witten, Axions In String Theory, *JHEP* **06** (), 051, [arXiv:hep-th/0605206](#).
 - [16] H.-Y. Schive, T. Chiueh, and T. Broadhurst, Cosmic Structure as the Quantum Interference of a Coherent Dark Wave, *Nature Phys.* **10**, 496 (2014), [arXiv:1406.6586 \[astro-ph.GA\]](#).
 - [17] H.-Y. Schive, M.-H. Liao, T.-P. Woo, S.-K. Wong, T. Chi-

- ueh, T. Broadhurst, and W. Y. P. Hwang, Understanding the Core-Halo Relation of Quantum Wave Dark Matter from 3D Simulations, *Phys. Rev. Lett.* **113**, 261302 (2014), [arXiv:1407.7762 \[astro-ph.GA\]](#).
- [18] L. Hui, J. P. Ostriker, S. Tremaine, and E. Witten, Ultralight scalars as cosmological dark matter, *Phys. Rev. D* **95**, 043541 (2017), [arXiv:1610.08297 \[astro-ph.CO\]](#).
- [19] S. Chandrasekhar, Dynamical Friction. I. General Considerations: the Coefficient of Dynamical Friction, *Astrophys. J.* **97**, 255 (1943).
- [20] L. Lancaster, C. Giovanetti, P. Mocz, Y. Kahn, M. Lisanti, and D. N. Spergel, Dynamical Friction in a Fuzzy Dark Matter Universe, *JCAP* **01** (), 001, [arXiv:1909.06381 \[astro-ph.CO\]](#).
- [21] N. Glennon, N. Musoke, E. O. Nadler, C. Prescod-Weinstein, and R. H. Wechsler, Dynamical friction in self-interacting ultralight dark matter, *Phys. Rev. D* **109**, 063501 (2024), [arXiv:2312.07684 \[astro-ph.CO\]](#).
- [22] Y. Wang and R. Easther, Dynamical friction from ultralight dark matter, *Phys. Rev. D* **105**, 063523 (2022), [arXiv:2110.03428 \[gr-qc\]](#).
- [23] R. Boey, Y. Wang, E. Kendall, and R. Easther, Dynamical friction and black holes in ultralight dark matter solitons, *Phys. Rev. D* **109**, 103526 (2024), [arXiv:2403.09038 \[astro-ph.CO\]](#).
- [24] L. Annulli, V. Cardoso, and R. Vicente, Response of ultralight dark matter to supermassive black holes and binaries, *Phys. Rev. D* **102**, 063022 (2020), [arXiv:2009.00012 \[gr-qc\]](#).
- [25] H. Koo, D. Bak, I. Park, S. E. Hong, and J.-W. Lee, Final parsec problem of black hole mergers and ultralight dark matter, *Phys. Lett. B* **856**, 138908 (2024), [arXiv:2311.03412 \[astro-ph.GA\]](#).
- [26] R. Boey, E. Kendall, Y. Wang, and R. Easther, Supermassive binaries in ultralight dark matter solitons, *Phys. Rev. D* **112**, 023510 (2025), [arXiv:2504.16348 \[astro-ph.CO\]](#).
- [27] M. Aghaie, G. Armando, A. Dondarini, and P. Panci, Bounds on ultralight dark matter from NANOGrav, *Phys. Rev. D* **109**, 103030 (2024), [arXiv:2308.04590 \[astro-ph.CO\]](#).
- [28] S. Tiruvaskar and C. Gordon, Self-Interacting Dark-Matter Spikes and the Final-Parsec Problem: Bayesian constraints from the NANOGrav 15-Year Gravitational-Wave Background, (2025), [arXiv:2506.18153 \[astro-ph.CO\]](#).
- [29] H. Lazare, J. Flitter, and E. D. Kovetz, Constraints on the fuzzy dark matter mass window from high-redshift observables, *Phys. Rev. D* **110**, 123532 (2024), [arXiv:2407.19549 \[astro-ph.CO\]](#).
- [30] B. Schwabe, M. Gosenca, C. Behrens, J. C. Niemeyer, and R. Easther, Simulating mixed fuzzy and cold dark matter, *Phys. Rev. D* **102**, 083518 (2020), [arXiv:2007.08256 \[astro-ph.CO\]](#).
- [31] B. C. Bromley, P. Sandick, and B. Shams Es Haghi, Supermassive black hole binaries in ultralight dark matter, *Phys. Rev. D* **110**, 023517 (2024), [arXiv:2311.18013 \[astro-ph.GA\]](#).
- [32] H.-Y. Schive, T. Chiueh, and T. Broadhurst, Soliton Random Walk and the Cluster-Stripping Problem in Ultralight Dark Matter, *Phys. Rev. Lett.* **124**, 201301 (2020), [arXiv:1912.09483 \[astro-ph.GA\]](#).
- [33] D. D. Chowdhury, F. C. van den Bosch, V. H. Robles, P. van Dokkum, H.-Y. Schive, T. Chiueh, and T. Broadhurst, On the Random Motion of Nuclear Objects in a Fuzzy Dark Matter Halo, *Astrophys. J.* **916**, 27 (2021), [arXiv:2105.05268 \[astro-ph.GA\]](#).
- [34] G. Agazie *et al.* (NANOGrav), The NANOGrav 15 yr Data Set: Constraints on Supermassive Black Hole Binaries from the Gravitational-wave Background, *Astrophys. J. Lett.* **952**, L37 (2023), [arXiv:2306.16220 \[astro-ph.HE\]](#).
- [35] G. Girelli, L. Pozzetti, M. Bolzonella, C. Giocoli, F. Marulli, and M. Baldi, The stellar-to-halo mass relation over the past 12 gyr: I. standard Λ cdm model, *Astronomy & Astrophysics* **634**, A135 (2020).
- [36] B. Schwabe, J. C. Niemeyer, and J. F. Engels, Simulations of solitonic core mergers in ultralight axion dark matter cosmologies, *Phys. Rev. D* **94**, 043513 (2016), [arXiv:1606.05151 \[astro-ph.CO\]](#).
- [37] P. Mocz, M. Vogelsberger, V. H. Robles, J. Zavala, M. Boylan-Kolchin, A. Fialkov, and L. Hernquist, Galaxy formation with BECDM – I. Turbulence and relaxation of idealized haloes, *Mon. Not. Roy. Astron. Soc.* **471**, 4559 (2017), [arXiv:1705.05845 \[astro-ph.CO\]](#).
- [38] L. E. Padilla, T. Rindler-Daller, P. R. Shapiro, T. Matos, and J. A. Vázquez, Core-Halo Mass Relation in Scalar Field Dark Matter Models and its Consequences for the Formation of Supermassive Black Holes, *Phys. Rev. D* **103**, 063012 (2021), [arXiv:2010.12716 \[astro-ph.GA\]](#).
- [39] A. Burkert, Fuzzy Dark Matter and Dark Matter Halo Cores, *Astrophys. J.* **904**, 161 (2020), [arXiv:2006.11111 \[astro-ph.GA\]](#).
- [40] M. Nori and M. Baldi, Scaling relations of fuzzy dark matter haloes – I. Individual systems in their cosmological environment, *Mon. Not. Roy. Astron. Soc.* **501**, 1539 (2021), [arXiv:2007.01316 \[astro-ph.CO\]](#).
- [41] M. Mina, D. F. Mota, and H. A. Winther, Solitons in the dark: First approach to non-linear structure formation with fuzzy dark matter, *Astron. Astrophys.* **662**, A29 (2022), [arXiv:2007.04119 \[astro-ph.CO\]](#).
- [42] A. Taruya and S. Saga, Analytical approach to the core-halo structure of fuzzy dark matter, *Phys. Rev. D* **106**, 103532 (2022), [arXiv:2208.06562 \[astro-ph.CO\]](#).
- [43] J. L. Zagarac, E. Kendall, N. Padmanabhan, and R. Easther, Soliton formation and the core-halo mass relation: An eigenstate perspective, *Phys. Rev. D* **107**, 083513 (2023), [arXiv:2212.09349 \[astro-ph.CO\]](#).
- [44] E. Kendall, M. Gosenca, and R. Easther, Aspherical ULDM collapse: variation in the core-halo mass relation, *Mon. Not. Roy. Astron. Soc.* **526**, 1046 (2023), [arXiv:2305.10340 \[astro-ph.CO\]](#).
- [45] G. Hinshaw, D. Larson, *et al.*, Nine-year wilkinson microwave anisotropy probe (wmap) observations: Cosmological parameter results, *Astrophys. J. Suppl. Ser.* **208**, 19 (2013).
- [46] G. Alonso-Álvarez, J. M. Cline, and C. Dewar, Self-interacting dark matter solves the final parsec problem of supermassive black hole mergers, *Phys. Rev. Lett.* **133**, 021401 (2024).
- [47] H. L. Child, S. Habib, K. Heitmann, N. Frontiere, H. Finkel, A. Pope, and V. Morozov, Halo Profiles and the Concentration–Mass Relation for a Λ CDM Universe, *Astrophys. J.* **859**, 55 (2018), [arXiv:1804.10199 \[astro-ph.CO\]](#).
- [48] A. Vehtari, A. Gelman, and J. Gabry, Practical bayesian model evaluation using leave-one-out cross-validation and waic, *Statistics and Computing* **27**, 1413–1432

- (2016).
- [49] A. Vehtari, D. Simpson, *et al.*, Pareto smoothed importance sampling (2024), [arXiv:1507.02646 \[stat.CO\]](#).
- [50] A. Gelman, J. Hwang, and A. Vehtari, Understanding predictive information criteria for bayesian models (2013), [arXiv:1307.5928 \[stat.ME\]](#).
- [51] R. Kumar, C. Carroll, A. Hartikainen, and O. Martin, Arviz a unified library for exploratory analysis of bayesian models in python, *Journal of Open Source Software* **4**, 1143 (2019).
- [52] M. Gosenca, A. Eberhardt, Y. Wang, B. Eggemeier, E. Kendall, J. L. Zagorac, and R. Easther, Multifield ultralight dark matter, *Phys. Rev. D* **107**, 083014 (2023), [arXiv:2301.07114 \[astro-ph.CO\]](#).